Nuclear magnetic field in Na$_{0.7}$CoO$_2$ detected with μ^-SR

Jun Sugiyama [1,2,3,*] Izumi Umegaki,[4] Soshi Takeshita,[3] Hiroya Sakurai,[5] Shoichiro Nishimura,[3] Ola Kenji Forslund,[6]
Elisabetta Nocerino,[6] Nami Matsubara,[6] Martin Månsson,[6] Takehito Nakano,[7] Ichihiro Yamauchi,[8]
Kazuhiko Ninomiya,[9] M. Kenya Kubo,[10] and Koichiro Shimomura[3]

[1]*Neutron Science and Technology Center, Comprehensive Research Organization for Science and Society (CROSS),
Tokai, Ibaraki 319-1106, Japan*
[2]*Advanced Science Research Center, Japan Atomic Energy Agency, Tokai, Ibaraki 319-1195, Japan*
[3]*High Energy Accelerator Research Organization (KEK), Tokai, Ibaraki 319-1106, Japan*
[4]*Toyota Central R&D Labs. Inc., Nagakute, Aichi 480-1192, Japan*
[5]*National Institute for Materials Science (NIMS), Namiki 1-1, Tsukuba, Ibaraki 305-0044, Japan*
[6]*Department of Applied Physics, KTH Royal Institute of Technology, SE-106 91 Stockholm, Sweden*
[7]*Institute of Quantum Beam Science, Graduate School of Science and Engineering, Ibaraki University, Mito, Ibaraki 310-8512, Japan*
[8]*Department of Physics, Graduate School of Science and Engineering, Saga University, Saga 840-8502, Japan*
[9]*Department of Chemistry, Graduate School of Science, Osaka University, Toyonaka, Osaka 560-0043, Japan*
[10]*College of Liberal Arts, International Christian University, Mitaka, Tokyo 181-8585, Japan*

The internal magnetic field in a sodium battery compound, i.e., the paramagnet Na$_{0.7}$CoO$_2$, was investigated with negative muon spin rotation and relaxation (μ^-SR), and the result was compared with the results previously obtained with μ^+SR. The majority of implanted μ^- is captured on an oxygen nucleus, while μ^+ locates an interstitial site. Therefore, a $\mu^\pm$SR work provides information on the internal magnetic field, which is formed by nuclear magnetic moments of ^{23}Na and ^{59}Co, from the two different viewpoints. Besides a slight decrease in the field distribution width (Δ) around 300 K, the nuclear magnetic field detected with μ^-SR was found to be almost static and temperature independent up to 400 K, even though Na ions are known to start to diffuse above 290 K based on μ^+SR, Na-NMR, neutron scattering, and electrochemical measurements. Such a discrepancy is caused by the fact that the Na contribution to Δ is only about 3% at the O site whereas it is about 13% at the interstitial site, where the μ^+ is presumably located.

I. INTRODUCTION

For energy materials research, it is often very imperative to know the dynamics of proton and/or alkali ions, such as Li$^+$, Na$^+$, and K$^+$, in materials and surfaces. For such purposes, nuclear magnetic resonance (NMR) is a common and a well-established technique [1], which detects fluctuation of a nuclear magnetic field induced by ion diffusion. However, NMR faces difficulty to estimate the diffusion coefficient for materials containing paramagnetic ions [2], due to the effect of paramagnetic spins on the spin-lattice relaxation rate ($1/T_1$). Instead, muon spin rotation and relaxation (μSR) was recently found to provide information on ion dynamics even in paramagnetic materials [3], because μSR distinguishes the internal magnetic field caused by nuclear magnetic moments ($H_{\mathrm{int}}^{\mathrm{N}}$) to that by electron magnetic moments ($H_{\mathrm{int}}^{\mathrm{E}}$) [4].

Since $H_{\mathrm{int}}^{\mathrm{N}}$ ranges below about 1/100 of $H_{\mathrm{int}}^{\mathrm{E}}$, the time domain for the former field observed with μSR is about

100 times slower than that for the latter field [5,6]. The muon spin precession frequency (f_μ) is connected with H_{int} at the muon site as $f_\mu = (\gamma_\mu/2\pi)H_{\mathrm{int}}$, where $\gamma_\mu/2\pi = 13.554$ kHz/Oe is the muon gyromagnetic factor. If one wants to measure $H_{\mathrm{int}}^{\mathrm{N}}$, the μSR spectrum should be recorded up to at least 10 μs with adequately high statistics. For the μSR using positive muons, i.e., μ^+SR, it is easily achieved to record a μ^+SR time spectrum up to 10 μs with, for instance, 10 Mevents statistics, because the counting rate in the current facilities ranges from 30 to 100 Mevents/h. Note that since the lifetime of a free $\mu^\pm$ is 2.196 μs, the number of the muons surviving until 10 μs decreases down to about 1%[$\sim \exp(-\frac{10}{2.196})$] of the total number of implanted muons.

On the other hand, the μSR using negative muons, i.e., μ^-SR, faces difficulty in obtaining data with the same accuracy as that of μ^+SR [7–11]. This is because the implanted spin-polarized μ^- is captured by a nucleus, resulting in the formation of a muonic atom. Additionally, the initial μ^- spin polarization is reduced down to about 1/6 during the cascade of the μ^- from the outermost shell orbit to the inner orbits of the muonic atom [12], whereas the μ^+ stops almost 100% spin polarized at the interstitial site in the lattice. Therefore, the asymmetry of μ^-SR is naturally decreased down to about 1/6 of that of μ^+SR, meaning that μ^-SR measurements require 36 times higher statistics than that for μ^+SR. As a result,

μ^-SR measurements need much longer collection times and cannot be completed within a typical beam time, i.e., below a week. However, the recent progress in pulsed muon facilities [13], such as the increase in the number of the incoming μ^- and the development of multidetector counting systems [14], drastically increases the counting rate of μ^-SR, which now enables us to study H_{int}^N with μ^-SR as well.

Concerning the muon site in the lattice, the implanted μ^+ is located at an interstitial site where the electrostatic potential is minimal, while the implanted μ^- is captured by a nucleus. As a result, the obtained information with μ^-SR is different from that obtained with μ^+SR. Such a difference is in principle very important for deeply understanding the physics in target materials.

Following upon the initial attempts to study H_{int}^N with μ^-SR for MgH_2 [15] and $LiMnPO_4$ [16], we have selected $Na_{0.7}CoO_2$ as the next target material. Within condensed matter physics, this material has several interests: It was originally studied as a cathode material for Na-ion batteries [17–19], and then attracted attention due to its good thermoelectric performance [20,21], and was used as a parent material for the hydrated superconductor $Na_{0.35}CoO_2 * 1.3H_2O$ [22]. Since the Co ions form a two-dimensional triangular lattice in the Na_xCoO_2 structure, the microscopic magnetic nature of Na_xCoO_2 was heavily investigated with μ^+SR [23–30], NMR [31–36], and neutron scattering [37–39] to understand the effect of geometrical frustration on the above properties and the diffusive nature of Na. However, μ^-SR investigations on this interesting compound still need to be performed.

The magnetic nature of Na_xCoO_2, prepared by a solid state reaction technique, is reported to depend on the Na content (x) [24,25,40]. The $x = 0.7$ sample exhibits a paramagnetic metallic behavior down to 1.8 K, while samples with $x = 0.74$–0.78 pose an antiferromagnetic (AF) transition around $T_N = 22$ K. A recent μ^+SR work on the $x = 0.7$ sample [41], which was prepared by an electrochemical reaction between the paramagnetic $Na_{0.7}CoO_2$ prepared by a solid state reaction technique and Na metal, reported the appearance of an AF phase below 22 K. This implies the importance of the Na distribution and vacancy order in the lattice, although the details are still unknown. In this μ^-SR work, we have used the paramagnetic $Na_{0.7}CoO_2$ sample prepared by a solid state reaction technique, since the Na_xCoO_2 sample with $T_N = 22$ K is not stable in air.

II. EXPERIMENT

A powder sample of $Na_{0.7}CoO_2$ was prepared at the National Institute for Materials Science (NIMS) using the solid state reaction technique reported in Ref. [42]. Here, a stoichiometric mixture of Na_2CO_3 (99.99%) and Co_3O_4 (99.9%), which were dried at 300 °C before use, was pressed into a pellet. The pellet was then placed in a dense alumina crucible and heated three times at 800, 850, and 950 °C for 6 h in an oxygen gas flow with intermediate grindings. The sample was characterized by a powder x-ray diffraction (XRD) analysis and magnetization measurements with a superconducting quantum interference device (SQUID) magnetometer [magnetic property measurement system (MPMS), Quantum Design], as seen in Fig. 1.
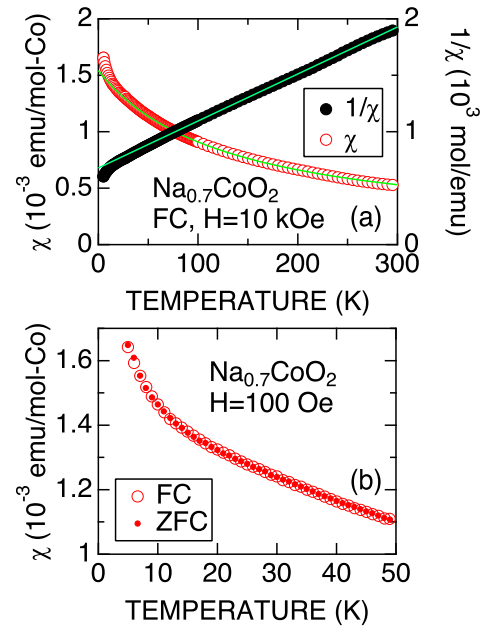

FIG. 1. The temperature dependencies of (a) magnetic susceptibility ($\chi = M/H$) and inverse susceptibility ($1/\chi = H/M$) recorded under a magnetic field $H = 10$ kOe and (b) χ recorded under $H = 100$ Oe for $Na_{0.7}CoO_2$. Magnetization (M) was measured in both a field-cooling (FC) mode and zero-field-cooling (ZFC) mode. In (a), green solid lines represent the best fit using a Curie-Weiss law, $\chi = \chi_0 + C(T - \Theta)$, in the temperature range between 50 and 250 K. Such a fit provides that $C = 0.186(2)$ emu K/mol Co and $\Theta = -128.5(1.6)$ K, leading to $\mu_{eff} = 1.218(8)\mu_B$/Co. These values are comparable to the values in Ref. [42], that is, $C = 0.16$ emu K/mol Co, $\Theta \sim -120$ K, and $\mu_{eff} \sim 1.1\mu_B$/Co. In (b), there is no clear anomaly in the $\chi^{FC}(T)$ and $\chi^{ZFC}(T)$ curves below 50 K, indicating the absence of an AF phase.

The μ^-SR time spectra were measured on the decay muon beam line D1 at MUSE of MLF J-PARC in Japan. An approximately 28-g powder sample was placed in a copper case with 15 cm^3 volume (3.6 cm $\phi \times 1.5$ cm), made of a 0.5-mm-thick Cu plate. The copper case was then set onto the bottom of the sample holder of a He-flow cryostat. The momentum of the μ^- beam was adjusted to 40 MeV/c to maximize the number of μ^- stopped in the sample. In order to increase the counting rate, a double-pulse muon beam was used for the measurements, where each pulse width is 100 ns and the second pulse follows the first pulse with a delay of 600 ns. The repetition rate of one set of the double pulses is 25 Hz, i.e., pulse on for 100 ns, off for 500 ns, on for 100 ns, and then off for 40 ms to the next double pulse [43]. The μ^-SR time spectrum was measured at temperatures between 100 and 450 K with up to 60 Mevents for transverse-field (TF) μ^-SR and 150 Mevents for zero-field (ZF) and longitudinal-field (LF) μ^-SR with a counting rate of about 30 Mevents/h. Here, TF (LF) means the field perpendicular (parallel) to the initial μ^- spin polarization. The experimental techniques are described in more detail elsewhere [5,6]. The obtained μSR data were analyzed with the MUSRFIT software package [44].
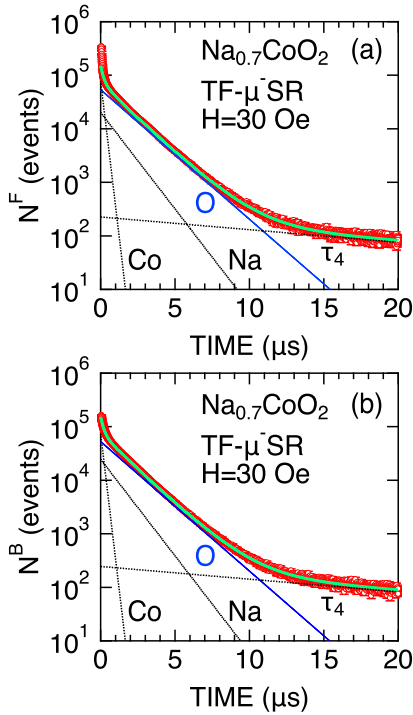
FIG. 2. The time histogram of the TF-μ^-SR spectrum in Na$_{0.7}$CoO$_2$ for the (a) forward (F) counter and (b) backward (B) counter. Red open circles represent the experimental data, green solid lines represent the fit result using Eq. (1), and the dominant O process is shown as a blue line whereas the minor ones, including the fourth unknown process, are in black dotted lines.

III. RESULTS

Figure 2 shows the time histograms of the forward and backward counters [$N^F(t)$ and $N^B(t)$] recorded in TF with $H = 30$ Oe. Here, forward (backward) means upstream (downstream) from the sample with respect to the μ^- beam. Since the decay asymmetry is very small and the lifetime of the μ^- depends on the nucleus it is captured on, the histogram of μ^-SR was fitted by a combination of four different decay processes,

$$N(t) = \sum_{i=1}^{n=4} N_i e^{-t/\tau_i}[1 + A_i e^{-\lambda_i t}\cos(\omega_i t + \phi_i)], \quad (1)$$

where N_i is a normalization constant at $t = 0$ for the ith decay process, τ_i is the corresponding muon lifetime for that process, A_i is the average muon decay asymmetry for that process, ω_i is

the angular frequency of the μ^- spin precession caused by the applied TF, and ϕ_i is the initial phase. As a first approximation, A_i is nonzero only for the predominant process and zero for the other minor processes.

The time histogram is well fitted with the nuclear capture processes of each element present in Na$_{0.7}$CoO$_2$ together with one more long life component (see Fig. 2 and Table I), as in the previous μ^-SR experiments [15]. The first decay process with $\tau_O = 1.7954$ μs is predominant in the time domain between 0.5 and 10 μs, where τ_O means τ for μ^- captured on ^{16}O [45]. The second and third decay processes represent muons captured on ^{23}Na with $\tau_{Na} = 1.204$ μs and ^{59}Co with $\tau_{Co} = 0.1858$ μs [45]. Since τ_4 [$= 18.6(5)$ μs] is longer than τ for a free $\mu^\pm$ (2.196 μs), the fourth decay process is caused by particles, such as e^- and/or neutrons or some other unknown effects. Fortunately, the contribution of the fourth decay process is negligibly small at $t \lesssim 10$ μs.

For the second and third processes, since the natural abundances of both ^{23}Na with $I = 3/2$ and ^{59}Co with $I = 7/2$ are 100%, the μ^- spins captured on Na and Co are rapidly depolarized due to a strong hyperfine interaction with the nuclear spin. In fact, the past μ^-SR work on Na metal [46,47] reported that $A_{Na} = 0.0090(15)$ and $\lambda_{Na} = 13.7(2.2)$ μs^{-1} at room temperature. λ_{Co} was also predicted to 1300 μs^{-1} [12]. Therefore, we could safely approximate the normalized asymmetry as the asymmetry solely from μ^- captured on O,

$$A_0 P(t) \sim \frac{N^B(t) - \alpha_O N^F(t)}{N^B(t) + \alpha_O N^F(t)}, \quad (2)$$

where A_0 is the initial ($t = 0$) asymmetry, $P(t)$ is the muon spin polarization function, and $\alpha_O \equiv N_O^B/N_O^F$. Here, since the initial μ^- (μ^+) spin is parallel (antiparallel) to its momentum, the numerator of the asymmetry is $N^B(t) - \alpha N^F(t)$ for μ^-SR [$N^F(t) - \frac{1}{\alpha}N^B(t)$ for μ^+SR].

Figures 3(a) and 3(b) show the TF-, ZF-, and LF-μ^-SR asymmetry spectra recorded at 100 and 390 K, respectively. At both temperatures, the ZF- and LF-μ^-SR spectra exhibit almost a static Kubo-Toyabe behavior, indicating that H_{int} is formed by random but roughly static nuclear magnetic moments. Thus, the ZF- and LF-μ^-SR spectra were fitted by a dynamic Gaussian Kubo-Toyabe signal (G^{DGKT}),

$$A_0 P(t) = A_{KT} G^{DGKT}(t, \Delta^-, \nu^-, H_{LF}), \quad (3)$$

where A_{KT} is the asymmetries associated with the signals from the μ^- captured on O, Δ^- is the static width of the nuclear field distribution at the μ^- sites, and ν^- is the fluctuation rate of the nuclear fields. Δ^- roughly corresponds to the spin-spin

TABLE I. Parameters of the TF-μ^-SR histograms for the Na$_{0.7}$CoO$_2$ sample obtained by fitting with Eq. (1), where τ_O, τ_{Na}, and τ_{Co} were fixed at the values reported in Ref. [45]. Since it is extremely difficult to determine short τ components using data at early times due to the effect of beam $e^\pm$ hitting the counters directly, the histograms were fitted only in the time domain between 0.4 and 16 μs.

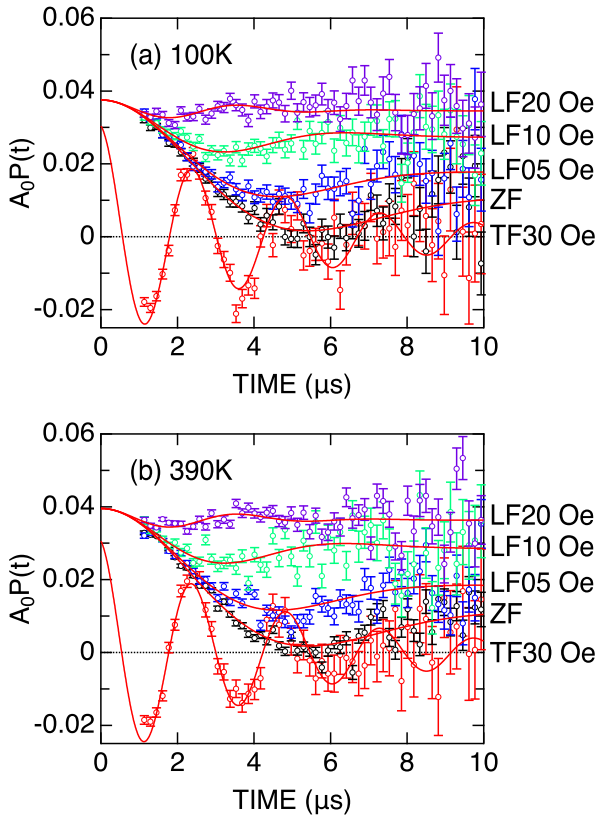| n	Component	τ (μs)	N_i^F/N_O^F	N_i^B/N_O^B	$\alpha_i \equiv N_i^B/N_i^F$	α_i/α_O
1	O	$\tau_O = 1.7954$[a]	1	1	$\alpha_O = 0.983(3)$	1
2	Na	$\tau_{Na} = 1.204$[a]	0.377(2)	0.467(8)	$\alpha_{Na} = 1.216(19)$	1.23(2)
3	Co	$\tau_{Co} = 0.1858$[a]	1.47(10)	1.42(4)	$\alpha_{Co} = 0.94(4)$	0.96(4)
4	?	$\tau_4 = 18.6(5)$	0.0042(2)	0.00465(10)	$\alpha_4 = 1.09(3)$	1.11(3)

[a]From Ref. [45].

FIG. 3. The TF-, ZF-, and LF-μ^-SR asymmetry spectra for Na$_{0.7}$CoO$_2$ recorded at (a) $T = 100$ K and (b) $T = 390$ K. Solid lines represent the best fit in the time domain between 1.2 and 10 μs using Eq. (3). The TF-μ^-SR spectrum was fitted by an exponentially relaxing cosine function, $A_0P(t) = A_{\mathrm{TF}} \exp(-\lambda_{\mathrm{TF}}t) \cos(2\pi f_{\mathrm{TF}}t + \phi_{\mathrm{TF}})$. Since we used a double-pulse beam, the asymmetry of the transverse field (TF) spectrum is smaller than those of the ZF and LF spectra due to an overlap of the two cosine signals with different initial phases. The data points between 0 and 1 μs are deleted due to the distortion of the spectrum caused by the double-pulse beam and the effect of the short lifetime components, i.e., τ_{Na} and τ_{Co} components.

relaxation rate ($1/T_2$) and ν^- the spin-lattice relaxation rate ($1/T_1$) [5,6]. For $\nu^- = H_{\mathrm{LF}} = 0$ (i.e., static and ZF), G^{DGKT} is equivalent to a *static* Gaussian Kubo-Toyabe function [48], which is expressed as

$$G_{zz}^{\mathrm{KT}}(t, \Delta^-) = \tfrac{1}{3} + \tfrac{2}{3}[1 - (\Delta^-)^2 t^2] \exp\left[-\tfrac{1}{2}(\Delta^-)^2 t^2\right]. \quad (4)$$

Although a nonlinear background signal was observed in the μ^-SR asymmetry spectrum for MgH$_2$ [15] and LiMnPO$_4$ [16], such a background signal is absent in the present spectrum (see Fig. 3). This is because $\alpha_4 (\equiv N_4^{\mathrm{B}}/N_4^{\mathrm{F}})$ for the τ_4 component, which is responsible for the nonlinear background signal, is close to $\alpha_{\mathrm{O}} (\equiv N_{\mathrm{O}}^{\mathrm{B}}/N_{\mathrm{O}}^{\mathrm{F}})$ for the τ_{O} component (see Table I). As a result, the normal asymmetry based on the O component reduces the nonlinear effect of the τ_4 component to the background signal. Since the τ_4 component was observed in the μ^-SR time histogram regardless of the sample, sample case, and facility [15,16], such a component is most likely included in the μ^- beam. That is, the μ^- captured on a

beam-line component (metals or alloys) produces unstable muonic atoms, which decay into long lifetime particles. Therefore, it is important to tune the beam to minimize the τ_4 component, but to maximize the other components.

In principle, α_{O} is equivalent to α_{Na} and α_{Co}, because the decay electron of each component comes from the μ^- captured in the Na$_{0.7}$CoO$_2$ sample. Since we used a double-pulse beam in this experiment, it is difficult to determine the correct t_0 (the timing that $t = 0$), which N_i seriously depends on, particularly for a short lifetime component. As a result, both α_{Na} and α_{Co} are slightly different from α_{O}. However, considering the lifetime and strong hyperfine interaction of the Na and Co components, they do not affect the asymmetry spectrum in the time domain at $t > 1$ μs.

IV. DISCUSSION

A simultaneous fit for the ZF- and LF-μ^-SR spectra using common Δ^- and ν^- in the time domain between 1.2 and 10 μs provided that $\Delta^- = 0.310(4)$ μs^{-1}, which corresponds to 3.65(4) Oe, and $\nu^- = 0.018(12)$ μs^{-1} at 100 K. Since dipole field calculations with DIPELEC [49] predict that $\Delta^{-,\mathrm{calc}} = 0.483$ μs^{-1}($= 5.67$ Oe) at the O site in Na$_{0.7}$CoO$_2$, so that $\Delta^-/\Delta^{-,\mathrm{calc}} \sim 2/3$. Such a discrepancy is probably caused by the increase in the bond length between Co and muonic O, due to a weak attractive force between the Co cation and the muonic O. In order to explain such a discrepancy, the required increase in the bond length is roughly estimated as 14%–17%, together with the local elongation of the lattice. The observed Δ^- is also affected by the uncertainty of t_0 and the accuracy of LF. However, the estimation error due to such factors is below 10%. Note that, since the field fluctuation rate (ν^-) is very small, the effect of the localized Co-3d moments on the dynamics of $H_{\mathrm{int}}^{\mathrm{N}}$ at the μ^- site is almost zero at 100 K.

Figure 4(a) shows the temperature dependencies of Δ^- and ν^- for Na$_{0.7}$CoO$_2$ determined with μ^-SR measurements. As expected from the ZF- and LF-μ^-SR spectra, Δ^- is roughly temperature independent up to about 400 K, although a small steplike decrease is observed between 300 and 340 K. As temperature increases from 100 K, ν^- slightly increases up to 300 K, then ν^- decreases with further increasing temperature. Since magnetization exhibits a Curie-Weiss behavior (see Fig. 1), the increase in ν^- above 100 K is naturally assigned as a dynamic behavior of $H_{\mathrm{int}}^{\mathrm{N}}$, as discussed below. However, the change in Δ^- and ν^- due to Na diffusion is rather small compared with those obtained with μ^+SR [26]. As seen in Table II, dipole field calculations with DIPELEC [49] predict that Δ^- for Na$_{0.7}$CoO$_2$ is 5.71 Oe, while Δ^- for Na$_0$CoO$_2$ is 5.54 Oe. Thus, the contribution of Na nuclei to Δ^- is found to be about 3%, because of the longer bond length of Na-O (2.391 Å) compared to Co-O (1.912 Å). In addition, for the μ^- captured on O, the number of the nearest-neighboring Na ions is 2.1, whereas the number of the Co ions is 3. Therefore, the slight change in Δ^- observed above 300 K reasonably corresponds to the expected decrease in Δ^- due to a motional narrowing by Na diffusion. Furthermore, 97% of $H_{\mathrm{int}}^{\mathrm{N}}$ are formed by Co nuclei, leading to a static nature even above 300 K. As a result, Na diffusion in Na$_{0.7}$CoO$_2$ is eventually invisible with μ^-SR.
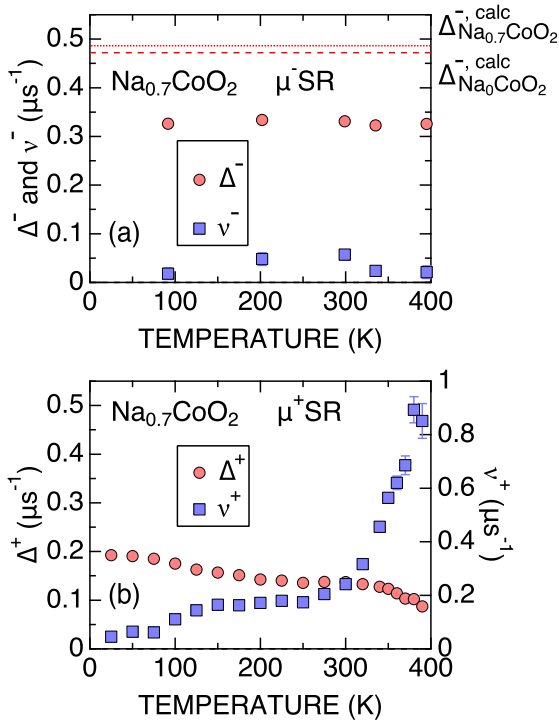
FIG. 4. The temperature dependencies of $\Delta^{\pm}$ and $\nu^{\pm}$ for Na$_{0.7}$CoO$_2$ determined with (a) μ^-SR and (b) μ^+SR [26]. The μ^-SR data were obtained by fitting the ZF- and LF-μ^-SR spectra with Eq. (3), while the μ^+SR data were obtained by fitting the ZF- and LF-μ^+SR spectra with $A_0P(t) = A_{\text{KT}}G^{\text{DGKT}}(t, \Delta^+, \nu^+, H_{\text{LF}}) + A_{\text{BG}}$, where the A_{BG} signal comes from the sample cell made of titanium (see Ref. [26]). In (a), the horizontal red dotted and dashed lines show the predicted Δ^- for Na$_{0.7}$CoO$_2$ and Na$_0$CoO$_2$ with dipole field calculations with DIPELEC [49]. Δ^+ for NaCoO$_2$ and Na$_0$CoO$_2$ are predicted as 0.494 and 0.428 μs^{-1} (5.806 and 5.028 Oe), respectively. The discrepancy of Δ^+ between the prediction and experiment is caused by difficulty in calculating the μ^+ site in the nonstoichiometric Na$_{0.7}$CoO$_2$ lattice (see text).

Such a slight change in Δ^- could be explained by the structural change in Na$_{0.7}$CoO$_2$. In fact, the previous neutron diffraction study [39] clarified that Na$_{0.7}$CoO$_2$ undergoes successive structural phase transitions from a low-temperature monoclinic phase to a medium-temperature orthorhombic

TABLE II. The field distribution width at the O site (Δ^-) in Na$_x$CoO$_2$ with $x = 0.7$ and 0 in the three phases, i.e., a low-temperature monoclinic phase at 50 K, a medium-temperature orthorhombic phase at 320 K, and a high-temperature hexagonal phase at 450 K. Δ^- was predicted by dipole field calculations with DIPELEC using the structural data in Ref. [39]. The lattice parameters of Na$_0$CoO$_2$ were assumed to be the same as those of Na$_{0.7}$CoO$_2$.

Phase	Na content (x)	Δ^- (Oe)	Δ^- (μs^{-1})
Monoclinic	0.7	5.708	0.4861
(at 50 K)	0	5.540	0.4718
Orthorhombic	0.7	5.708	0.4861
(at 320 K)	0	5.542	0.4720
Hexagonal	0.7	5.673	0.4831
(at 450 K)	0	5.507	0.4690

phase at $T_{c1} \sim 290$ K and to a high-temperature hexagonal phase at $T_{c2} \sim 400$ K. Table II summarizes Δ^- for each phase predicted by dipole field calculations. This shows that Δ^- in the monoclinic phase (Δ^-_{mono}) is almost equivalent to Δ^- in the orthorhombic phase (Δ^-_{ortho}). Considering a small thermal variation of the lattice parameters of the monoclinic phase [39], $\Delta^-_{\text{mono}}(50\text{ K})$ is very close to $\Delta^-_{\text{mono}}(290\text{ K})$. Therefore, it is highly unlikely that the structural phase transition at T_{c1} induces the slight change in Δ^- around 300 K.

The previous μ^+SR measurements on Na$_{0.7}$CoO$_2$ [26] provided more remarkable temperature dependencies of Δ^+ and ν^+ [see Fig. 4(b)]. As temperature increases from 25 K, Δ^+ decreases slowly up to around 300 K, and decreases more rapidly with further increasing temperature. Furthermore, ν^+ increases slowly with temperature up to 300 K, and rapidly increases with further increasing temperature. These behaviors unambiguously demonstrate the Na diffusion above 300 K in Na$_{0.7}$CoO$_2$, because such a diffusive nature has been confirmed with Na-NMR [33], neutron diffraction [39], and electrochemical measurements [50]. In fact, the $\nu^+(T)$ is very consistent with the spin-lattice relaxation ($1/T_1$)-vs-T curve obtained from Na-NMR [33]. This clearly excludes the scenario that μ^+ is diffusing above 300 K, but supports the scenario that immobile μ^+ senses Na diffusion. Since the implanted μ^+ locate the interstitial site in the Na$_{0.7}$CoO$_2$ lattice, which is naturally more proximate to the Na ions than the O site, μ^+SR is more sensitive to Na diffusion than μ^-SR in Na$_{0.7}$CoO$_2$. If we assume the μ^+ site as (2/3, 1/3, 0.1010) in the NaCoO$_2$ lattice based on density functional theory (DFT) calculations with a VASP code package [51], the contribution of Na nuclei to Δ^+ is about 13%, being consistent with the present results. Note that it is impossible to predict the μ^+ site in the nonstoichiometric Na$_{0.7}$CoO$_2$ lattice by the present DFT calculations. Instead, the μ^+ site was predicted to be (2/3, 1/3, 0.1010) for NaCoO$_2$ and (1/3, 2/3, 1/4) for Na$_0$CoO$_2$, i.e., a vacant Na site. The μ^+ site is thus expected to shift gradually from (2/3, 1/3, 0.1010) to (1/3, 2/3, 1/4) with decreasing Na content. Therefore, as the Na content decreases, Δ^+ decreases but the contribution of Na nuclei to Δ^+ increases from the above estimation for NaCoO$_2$ ($\sim$13%) due to the simultaneous elongation of the Co-μ^+ distances and contraction of the Na-μ^+ distances.

Back to the $\nu^{\pm}(T)$ curve below 300 K, the μ^-SR result is similar to the μ^+SR result (a slow increase seen in Fig. 4), implying the essential change in the local magnetic environments of both Co and Na with temperature. In fact, the past Co-NMR [31,32] and Na-NMR [33–35] work also revealed an increase in the spin-lattice relaxation rate ($1/T_1$) with temperature below 300 K. The change in the Co environment is most likely caused by charge ordering and/or charge instability of the Co ions in the CoO$_2$ layer [32,36], for details that are still not clarified. Recent neutron work on Na$_{0.7}$CoO$_2$ [39] showed that Na$^+$ ions start to change the position slowly above 200 K, leading to a structural phase transition at 290 K. This implies that the Co valence state and/or distribution would be affected by such Na motion.

V. SUMMARY

In summary, we have observed a nuclear magnetic field (H_{int}^{N}) in Na$_{0.7}$CoO$_2$ with μ^-SR as a function of temperature

up to 400 K. Since μ^-SR mainly detected $H_{\text{int}}^{\text{N}}$ formed by Co, the obtained result showed an almost static behavior in the whole temperature range measured. However, a small change in the field fluctuation rate at temperatures between 100 and 300 K indicated the change in the Co state associated with the Na movement. Due to the difference of the sites between μ^- and μ^+ in the $Na_{0.7}CoO_2$ lattice, μ^-SR mainly provided microscopic magnetic information related to the Co environment, while μ^+SR results provided information on both Co and Na. The current study is an example of how μ^-SR and μ^+SR can compliment each other by probing the internal field from different lattice sites.

[1] C. Vinod Chandran and P. Heitjans, *Solid-State NMR Studies of Lithium Ion Dynamics Across Materials Classes*, in *Annual Reports on NMR Spectroscopy* (Academic, New York, 2016), Vol. 89, pp. 1–102.

[2] C. P. Grey and N. Dupré, Chem. Rev. **104**, 4493 (2004).

[3] J. Sugiyama, K. Mukai, Y. Ikedo, H. Nozaki, M. Månsson, and I. Watanabe, Phys. Rev. Lett. **103**, 147601 (2009).

[4] J. Sugiyama, K. Mukai, M. Harada, H. Nozaki, K. Miwa, T. Shiotsuki, Y. Shindo, S. R. Giblin, and J. Lord, Phys. Chem. Chem. Phys. **15**, 10402 (2013).

[5] G. M. Kalvius, D. R. Noakes, and O. Hartmann, in *Handbook on the Physics and Chemistry of Rare Earths*, edited by K. A. Gschneidner, L. Eyring, Jr., and G. H. Lander (North-Holland, Amsterdam, 2001), Vol. 32, Chap. 206, pp. 55–451.

[6] A. Yaouanc and P. D. de Réotier, *Muon Spin Rotation, Relaxation, and Resonance, Application to Condensed Matter* (Oxford University Press, New York, 2011).

[7] S. Nagamiya, K. Nagamine, O. Hashimoto, and T. Yamazaki, Phys. Rev. Lett. **35**, 308 (1975).

[8] K. Nagamine, S. Nagamiya, O. Hashimoto, S. Kobayashi, and T. Yamazaki, Hyperfine Interact. **2**, 407 (1976).

[9] Y. Yoshida, T. Kobayashi, H. Nakayama, H. Yasuoka, and T. Yamazaki, Hyperfine Interact. **4**, 448 (1978).

[10] J. H. Brewer, Hyperfine Interact. **19**, 873 (1984).

[11] N. Nishida, Hyperfine Interact. **79**, 823 (1993).

[12] R. Winston, Phys. Rev. **129**, 2766 (1963).

[13] Y. Miyake, K. Shimomura, N. Kawamura, A. Koda, P. Strasser, K. M. Kojima, H. Fujimori, S. Makimura, Y. Ikedo, Y. Kobayashi, J. Nakamura, Y. Oishi, S. Takeshita, T. Adachi, A. D. Pant, H. Okabe, S. Matoba, M. Tampo, M. Hiraishi, K. Hamada *et al.*, JPS Conf. Proc. **21**, 011054 (2018).

[14] K. M. Kojima, T. Murakami, Y. Takahashi, H. Lee, S. Y. Suzuki, A. Koda, I. Yamauchi, M. Miyazaki, M. Hiraishi, H. Okabe, S. Takeshita, R. Kadono, T. Ito, W. Higemoto, S. Kanda, Y. Fukao, N. Saito, M. Saito, M. Ikeno, T. Uchida, and M. M. Tanaka, J. Phys.: Conf. Ser. **551**, 012063 (2014).

[15] J. Sugiyama, I. Umegaki, H. Nozaki, W. Higemoto, K. Hamada, S. Takeshita, A. Koda, K. Shimomura, K. Ninomiya, and M. K. Kubo, Phys. Rev. Lett. **121**, 087202 (2018).

[16] J. Sugiyama, O. K. Forslund, E. Nocerino, N. Matsubara, K. Papadopoulos, Y. Sassa, S. P. Cottrell, A. D. Hillier, K. Ishida, M. Månsson, and J. H. Brewer, Phys. Rev. Research **2**, 033161 (2020).

[17] J. Molenda, C. Delmas, and P. Hagenmuller, Solid State Ionics **9–10**, 431 (1983).

[18] L. W. Shacklette, J. Electrochem. Soc. **135**, 2669 (1988).

[19] R. Berthelot, D. Carlier, and C. Delmas, Nat. Mater. **10**, 74 (2011).

[20] J. Molenda, C. Delmas, P. Dordor, and A. Stokłosa, Solid State Ionics **12**, 473 (1984).

[21] I. Terasaki, Y. Sasago, and K. Uchinokura, Phys. Rev. B **56**, R12685(R) (1997).

[22] K. Takada, H. Sakurai, E. Takayama-Muromachi, F. Izumi, R. A. Dilanian, and T. Sasaki, Nature (London) **422**, 53 (2003).

[23] J. Sugiyama, H. Itahara, J. H. Brewer, E. J. Ansaldo, T. Motohashi, M. Karppinen, and H. Yamauchi, Phys. Rev. B **67**, 214420 (2003).

[24] J. Sugiyama, J. H. Brewer, E. J. Ansaldo, H. Itahara, T. Tani, M. Mikami, Y. Mori, T. Sasaki, S. Hébert, and A. Maignan, Phys. Rev. Lett. **92**, 017602 (2004).

[25] J. Sugiyama, J. H. Brewer, E. J. Ansaldo, B. Hitti, M. Mikami, Y. Mori, and T. Sasaki, Phys. Rev. B **69**, 214423 (2004).

[26] M. Månsson and J. Sugiyama, Phys. Scr. **88**, 068509 (2013).

[27] S. P. Bayrakci, C. Bernhard, D. P. Chen, B. Keimer, R. K. Kremer, P. Lemmens, C. T. Lin, C. Niedermayer, and J. Strempfer, Phys. Rev. B **69**, 100410(R) (2004).

[28] P. Mendels, D. Bono, J. Bobroff, G. Collin, D. Colson, N. Blanchard, H. Alloul, I. Mukhamedshin, F. Bert, A. Amato, and A. D. Hillier, Phys. Rev. Lett. **94**, 136403 (2005).

[29] G. Lang, J. Bobroff, H. Alloul, P. Mendels, N. Blanchard, and G. Collin, Phys. Rev. B **72**, 094404 (2005).

[30] J. Sugiyama, Y. Ikedo, M. Månsson, J. H. Brewer, S. L. Stubbs, E. J. Ansaldo, K. H. Chow, J. S. Lord, H. Ohta, C. Michioka, and K. Yoshimura, Phys. Rev. B **82**, 214505 (2010).

[31] F. L. Ning, T. Imai, B. W. Statt, and F. C. Chou, Phys. Rev. Lett. **93**, 237201 (2004).

[32] J. L. Gavilano, B. Pedrini, K. Magishi, J. Hinderer, M. Weller, H. R. Ott, S. M. Kazakov, and J. Karpinski, Phys. Rev. B **74**, 064410 (2006).

[33] J. L. Gavilano, D. Rau, B. Pedrini, J. Hinderer, H. R. Ott, S. M. Kazakov, and J. Karpinski, Phys. Rev. B **69**, 100404(R) (2004).

[34] Y. Ihara, K. Ishida, C. Michioka, M. Kato, K. Yoshimura, H. Sakurai, and E. Takayama-Muromachi, J. Phys. Soc. Jpn. **73**, 2963 (2004).

[35] P. Carretta, M. Mariani, C. B. Azzoni, M. C. Mozzati, I. Bradarić, I. Savić, A. Feher, and J. Šebek, Phys. Rev. B **70**, 024409 (2004).

[36] G. Lang, J. Bobroff, H. Alloul, G. Collin, and N. Blanchard, Phys. Rev. B **78**, 155116 (2008).

[37] S. P. Bayrakci, I. Mirebeau, P. Bourges, Y. Sidis, M. Enderle, J. Mesot, D. P. Chen, C. T. Lin, and B. Keimer, Phys. Rev. Lett. **94**, 157205 (2005).

[38] L. M. Helme, A. T. Boothroyd, R. Coldea, D. Prabhakaran, D. A. Tennant, A. Hiess, and J. Kulda, Phys. Rev. Lett. **94**, 157206 (2005).

[39] M. Medarde, M. Mena, J. L. Gavilano, E. Pomjakushina, J. Sugiyama, K. Kamazawa, V. Y. Pomjakushin, D. Sheptyakov, B. Batlogg, H. R. Ott, M. Månsson, and F. Juranyi, Phys. Rev. Lett. **110**, 266401 (2013).

[40] M. L. Foo, Y. Wang, S. Watauchi, H. W. Zandbergen, T. He, R. J. Cava, and N. P. Ong, Phys. Rev. Lett. **92**, 247001 (2004).

[41] Y. Sassa, I. Umegaki, H. Nozaki, O. Forslund, C. Delmas, J.-C. Orain, A. Amato, D. Andreica, M. Månsson, and J. Sugiyama, JPS Conf. Proc. **21**, 011019 (2018).

[42] H. Sakurai, S. Takenouchi, N. Tsujii, and E. Takayama-Muromachi, J. Phys. Soc. Jpn. **73**, 2081 (2004).

[43] P. Strasser, A. Koda, K. M. Kojima, T. U. Ito, H. Fujimori, Y. Irie, M. Aoki, Y. Nakatsugawa, W. Higemoto, M. Hiraishi, H. Li, H. Okabe, S. Takeshita, K. Shimomura, N. Kawamura, R. Kadono, and Y. Miyake, JPS Conf. Proc. **21**, 011061 (2018).

[44] A. Suter and B. Wojek, Phys. Proc. **30**, 69 (2012).

[45] T. Suzuki, D. F. Measday, and J. P. Roalsvig, Phys. Rev. C **35**, 2212 (1987).

[46] T. P. Gorringe, B. L. Johnson, D. S. Armstrong, J. Bauer, M. A. Kovash, M. D. Hasinoff, D. F. Measday, B. A. Moftah, R. Porter, and D. H. Wright, Phys. Rev. Lett. **72**, 3472 (1994).

[47] J. H. Brewer, K. Ghandi, A. M. Froese, and B. A. Fryer, Phys. Rev. C **71**, 058501 (2005).

[48] R. Kubo and T. Toyabe, *Magnetic Resonance and Relaxation* (North-Holland, Amsterdam, 1996).

[49] K. M. Kojima, J. Yamanobe, H. Eisaki, S. Uchida, Y. Fudamoto, I. M. Gat, M. I. Larkin, A. Savici, Y. J. Uemura, P. P. Kyriakou, M. T. Rovers, and G. M. Luke, Phys. Rev. B **70**, 094402 (2004).

[50] G. J. Shu and F. C. Chou, Phys. Rev. B **78**, 052101 (2008).

[51] G. Kresse and J. Hafner, Phys. Rev. B **47**, 558 (1993).